Multipolar contributions to electron self-energies: extreme tight binding model

2001 J. Phys.: Condens. Matter 13 1215

(http://iopscience.iop.org/0953-8984/13/6/303)

INSTITUTE OF PHYSICS PUBLISHING JOURNAL OF PHYSICS: CONDENSED MATTER

J. Phys.: Condens. Matter **13** (2001) 1215–1231 www.iop.org/Journals/cm PII: S0953-8984(01)14300-6

Multipolar contributions to electron self-energies: extreme tight binding model

Marco Nicastro, Svjetlana Galamic-Mulamerovic and Charles H Patterson

Department of Physics and Centre for Scientific Computation, University of Dublin, Trinity College, Dublin 2, Ireland

Received 30 May 2000, in final form 22 December 2000

Abstract

Discrete dipole models provide a means of calculating optical properties of semiconductor surfaces rapidly and quite accurately, but they are generally regarded as being purely phenomenological. A connection between such models and a quantum mechanical extreme tight binding (ETB) model is established here. The dielectric function obtained from an extreme tight binding model is shown to be of similar form to that of a model in which a solid is treated as a lattice of polarizable, pointlike entities, the discrete dipole model. The dielectric matrix is expressed in terms of its eigenvectors and eigenvalues, which are dipole waves and plasmon energies. The ETB dielectric matrix is used to derive the self-energy of valence and conduction band states in fcc argon. This results in a simple physical picture where intra- and inter-band scattering events result in virtual monopoles and dipoles on a lattice which couple to plasmon modes. The self-energies of electron and hole states of fcc argon are analysed in terms of multipolar contributions.

1. Introduction

Ab initio many-body calculations provide accurate results for single-particle and collective excitations in solids and have been reported in the literature for about 15 years [1]. Such calculations are still prohibitively expensive in computer time for systems with large unit cells, which can, however, be treated by less accurate methods for excitations such as density functionals. In this paper, two quantities encountered in many-body physics of solids, the self-energy and screened interaction, are analysed using extreme tight binding (ETB) and discrete dipole (DD) models. These models lend themselves to a clear understanding of the physics involved and means of improving application of many-body methods to large systems may be found once the relationship between classical dipole and quantum mechanical response functions is understood. Plasmon pole approximations for the inverse dielectric function are important in many-body calculations as they provide a means of obtaining the inverse dielectric function at finite frequencies from a single calculation of the static dielectric matrix. This paper shows that dipole wave eigenmodes from the DD model correspond to the plasmon

0953-8984/01/061215+17$30.00

modes obtained from an ETB calculation of the dielectric matrix and it presents an analysis of contributions of the various plasmon modes to the dielectric function in condensed argon. It is emphasized that the main purposes of this paper are: to provide an intuitive picture of processes leading to electron and hole self-energies and to illuminate the physical basis of discrete dipole models.

The discrete dipole model has a long history as a model for the dielectric response of insulating or semiconducting materials, beginning with Lorentz and Ewald [2], who formulated a method for calculating the lattice sums appearing in the model. Since then it has been applied to bulk solids [3], solid surfaces [4–10] and scattering of electromagnetic radiation by dust particles in space [11]. There are several other model dielectric functions for insulating and semiconducting materials in the literature [12–16], some of which are based on ETB approximations for the electronic structure of the material [13–15]. The model that we use to calculate the electron self-energy in insulators is similar to the electronic polaron model of Toyozawa [17]. The particular DD model considered here consists of dipole-polarizable sites placed at atom centres, coupled by point-dipolar electrostatic fields. The model gives a good account of the long wavelength dielectric function of bulk silicon [3] and anisotropies in the reflectivities of silicon surfaces [10]. Systems with unit cells containing over 100 silicon atoms and slabs over 80 Å thick with periodic boundary conditions parallel to the surface can be treated so that, for example, optical effects which persist many atomic layers into a solid surface can be studied.

In section 2 the DD and ETB models are outlined, the relationship between the response functions derived using these models is established and expressions for the screened interaction and GW self-energy are given within the ETB approximation. In section 3 dispersion relations for plasmon modes and ETB model self-energies in condensed argon are presented. Screening mechanisms are discussed in section 4 and a summary is given in section 5. A derivation of the ETB dielectric function is given in Appendix A and lattice sums are described in Appendix B.

2. Model dielectric functions

2.1. Definitions

The key quantities in a calculation of the self-energy of electronic states within the GW approximation [18, 19] are the inverse dielectric function, ε^{-1}, the response function, R, the screened interaction between charges, W, and the polarizability, P. Each of these is a two point function in space variables and is frequency dependent. When expressed in a basis, these functions become matrices whose elements depend on wavevector, $\boldsymbol{q}$, and frequency, ω. The dielectric function relates an external applied potential to the total potential, i.e. external potential plus induced potential, through the density response function or polarizability, P, and is given by [19]

$$\varepsilon = 1 - v\frac{\delta\rho}{\delta V^{tot}} = 1 - vP \tag{1}$$

where ρ is the induced charge density, V^{tot} is the total potential and v is the Coulomb interaction. The inverse dielectric function gives the response to an external potential and is [19]

$$\varepsilon^{-1} = 1 + v\frac{\delta\rho}{\delta\phi} = 1 + vR \tag{2}$$

where ϕ is an external potential and R is the response function. The polarizability and response function are related by

$$R = (1 - vP)^{-1}P = (P^{-1} - v)^{-1}. \tag{3}$$

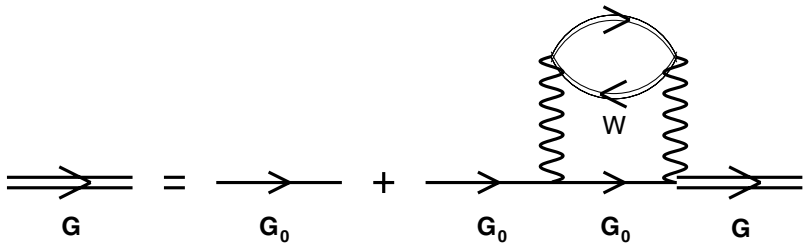

Figure 1. Diagrammatic representation of equation (5). In the rightmost diagram an electron undergoes an intra- or inter-band scattering event and polarizes the medium, which in turn reacts on the scattered electron.

Finally, the screened interaction between electric charges is

$$W = \varepsilon^{-1} v = v + vRv. \tag{4}$$

Single particle excitations in an interacting system [18] occur at the poles of the Green function of the interacting system. Dyson's equation for the Green function of the interacting system, G,

$$G = G_0 + G_0 \Sigma G \tag{5}$$

relates G to the Green function for the non-interacting system, G_0, and the self-energy, Σ. Feynman diagrams representing equation (5) are illustrated in figure 1. Hedin's GW approximation [18, 19] to the self-energy operator involves a frequency convolution of the Green function for the non-interacting system with the screened interaction so that $\Sigma = \mathrm{i}G_0 W$. Manipulation of equation (5) shows that

$$G = (G_0^{-1} - \Sigma)^{-1} \tag{6}$$

so that poles of G are shifted from poles of G_0 by Σ, which represents a correction to single particle excitation energies. In order to find these energy shifts, matrix elements of the self-energy operator with the state in question, Ψ_{ik}, must be calculated,

$$\Sigma_i(\boldsymbol{k}, \omega) = \langle \Psi_{ik} | \Sigma(\boldsymbol{r}, \boldsymbol{r}', \omega) | \Psi_{ik} \rangle. \tag{7}$$

In many GW calculations [1] a plane wave basis is used. However, the physical processes represented by this approximation become much clearer when a local orbital basis is used. These include induction of virtual charges in the material as an electron or hole scatters from state to state (figure 1) and screening of these charges by induction of dipole moments at sites neighbouring the virtual charges. The ETB model valence band consists of p states and the conduction band consists of s states. An electron in a valence band state, p_k, can scatter into a state p_{k+q}, emitting a 'photon' with momentum $\boldsymbol{q}$ and thereby interacting with the medium before scattering back into the original state. In scattering from one p state to another, the virtual charge is a density wave of 'p monopoles', i.e. $\mathrm{p}_k(\boldsymbol{r})^* \mathrm{p}_{k+q}(\boldsymbol{r}) \exp[\mathrm{i}\boldsymbol{q} \cdot \boldsymbol{R}]$ and it interacts with the medium through a screened $1/r$ potential. $\boldsymbol{R}$ is a lattice translation vector. An electron scattering from one s state to another induces a wave of 's monopoles' and also interacts with the medium through a screened $1/r$ potential. However, an electron in a p state scattering into an s state induces an 'sp dipole', i.e. $\mathrm{s}_k^*(\boldsymbol{r}) \mathrm{p}_{k+q}(\boldsymbol{r}) \exp[\mathrm{i}\boldsymbol{q} \cdot \boldsymbol{R}]$ and interacts with the medium through a screened $1/r^3$ potential. Thus the self-energy for an s or p state contains screened monopolar and dipolar interactions with the medium, and in general it will contain additional interactions with the medium describable in terms of higher multipoles.

2.2. Discrete dipole model

The DD model used by this group has been described in detail elsewhere [3] and only a brief summary is given here. The dipole induced at any site is determined by the polarizability and the local field,

$$\boldsymbol{p}_i(\omega) = \alpha_i(\omega) \cdot \boldsymbol{E}_i^{LOC} = \alpha_i(\omega) \cdot [\boldsymbol{E}_i^{A}(\omega) - \boldsymbol{t}_{ij} \cdot \boldsymbol{p}_j(\omega)] \tag{8}$$

where $\boldsymbol{p}_i(\omega)$ is the dipole moment at site i and $\alpha_i(\omega)$ is a frequency-dependent polarizability matrix for site i. In this work the polarizability is isotropic; in our earlier work, e.g. [3], a polarizability with a small anisotropy was used. The polarizability is

$$\alpha_i(\omega) = \frac{2e^2}{m((\omega_0 - \mathrm{i}\delta)^2 - \omega^2)}\boldsymbol{I} = e^2\alpha(\omega)\boldsymbol{I}. \tag{9}$$

$\boldsymbol{E}_i^{LOC}$ is the local field, which consists of an external field, $\boldsymbol{E}_i^{A}$, and a field created by all other dipoles in the system. $\boldsymbol{t}_{ij}$ is a 3×3 dipole–dipole interaction tensor which determines the contribution to the local field at site i due to a dipole at site j and $\boldsymbol{I}$ is the 3×3 unit matrix. m is an effective mass and ω_0 is the bare transition frequency of a bond or atom. When dipolar coupling of polarizable sites is taken into account, a set of normal modes can be obtained [3]. A bare transition energy of $\hbar\omega_0 = 14.3$ eV was used for argon [20].

In what follows we use the convention that if a subscripted site index is used with a vector or matrix, a single atom or covalent bond site is indicated but if no index is used then a composite vector or matrix describing a whole (finite) system or unit cell is indicated. We also adopt a notation where the dependence of any quantity, f, on wavevector, $\boldsymbol{q}$, may be indicated as $f(\boldsymbol{q})$ or f_q.

Equations (8) and (9) are suitable for treating a finite system, but when an infinite system is treated using periodic boundary conditions, site dipole moments are replaced by characteristic dipoles in the zeroth unit cell. Dipoles outside the zeroth unit cell, $\boldsymbol{p}_\lambda(\omega)$, are related to the characteristic dipoles, $\boldsymbol{p}_\lambda(\omega)$, by

$$\boldsymbol{p}_\lambda(\omega) = \boldsymbol{p}_{\boldsymbol{q}}(\omega)\exp[\mathrm{i}\boldsymbol{q} \cdot \boldsymbol{R}_\lambda] \tag{10}$$

where $\boldsymbol{R}_\lambda$ is a lattice vector connecting the two sites in the zeroth and λth unit cells. The local field at the ith characteristic dipole site caused by a wavelike excitation of dipoles at the site labelled j in each unit cell can be evaluated by a discrete Fourier transform of dipole–dipole interaction tensors, $\boldsymbol{t}(\boldsymbol{R}_\lambda)\exp[\mathrm{i}\boldsymbol{q} \cdot \boldsymbol{R}_\lambda] = \boldsymbol{T}_q$ [3]. In a lattice with no external field present, equation (8) becomes

$$\left[\left(\alpha^{-1}(0) - \frac{m\omega^2}{2e^2}\right)\boldsymbol{I} + \boldsymbol{T}_q\right] \cdot \boldsymbol{p}_q(\omega) = 0 \tag{11}$$

and free dipole oscillations are found at zeros of the determinant,

$$|(\alpha^{-1}(0) - \mu_{nq}^2)\boldsymbol{I} + \boldsymbol{T}_q|. \tag{12}$$

The response function for a bulk discrete dipole system can be expressed in terms of the characteristic dipoles and the eigenvalues and eigenvectors of the matrix in equation (11). The eigenvectors, $\boldsymbol{p}_{nq}$, are called dipole waves and have eigenfrequencies, Ω_{nq}, related to the eigenvalues of equation (12), μ_{nq}^2, by [3]

$$\Omega_{nq}^2 = 2e^2\mu_{nq}^2/m. \tag{13}$$

It is convenient for later sections to express eigenvector characteristic dipoles as charges times displacement from equilibrium, $\boldsymbol{p}_{nq} = 2e\boldsymbol{x}_{nq}$. The dipole response function, $\alpha(q, \omega)$, for a bulk discrete dipole system is defined by

$$\boldsymbol{p}(\boldsymbol{q}, \omega) = \alpha(\boldsymbol{q}, \omega) \cdot \boldsymbol{E}^{A}(\boldsymbol{q}, \omega) \tag{14}$$

where $\alpha(\boldsymbol{q}, \omega)$ is given by [3],

$$\alpha(\boldsymbol{q}, \omega) = \sum_n \frac{2e^2}{m} \frac{\boldsymbol{x}_{nq} \boldsymbol{x}_{nq}^{T^*}}{(\Omega_{nq} - \mathrm{i}\delta)^2 - \omega^2} = e^2 \boldsymbol{X}_q. \tag{15}$$

2.3. Extreme tight binding model

An ETB model is used to derive the dielectric function, response function, screened interaction and self-energy of a system with one site per cell. This is a model in which the quantum mechanical wavefunctions for the system are sufficiently localized on sites that there is no overlap between wavefunctions on different sites. Consequently there is no dispersion of eigenvalues associated with these states when such a model is used for a crystalline solid; there is a single valence band energy and a single conduction band energy in the ETB model for crystalline Ar. The overlap matrix in the ETB basis is a unit matrix. An approximation in the dielectric function derived below allows the response function and inverse dielectric matrix to be expressed in terms of dipole wave eigenvectors and eigenfrequencies, thereby making the connection between the two models.

As stated above, valence bands in this model are linear combinations of non-overlapping, Cartesian–Gaussian p orbitals located at the atom centre. Conduction bands are non-overlapping s orbitals at the same sites. Valence and conduction bands are normalized on one unit cell whose volume is denoted V. Hamiltonian matrix elements between orbitals on different sites are assumed to be zero and so linear combinations of *one* orbital type per primitive cell,

$$\Psi_{ik}(\boldsymbol{r}) = \sum_\lambda \chi_i(\boldsymbol{r} - \boldsymbol{R}_\lambda) \exp[\mathrm{i}\boldsymbol{k} \cdot \boldsymbol{R}_\lambda] \tag{16}$$

satisfy the Schrödinger equation. i is a site/orbital index ($i = 1, \ldots, 4$ refer to s, p_x, p_y, p_z), λ is a unit cell index and χ is an s or p orbital normalized on the unit cell. These eigenfunctions are also used as expansion functions for the Coulomb interaction, etc. A 2×2 matrix notation is used to represent the 4×4 matrix of expansion coefficients for these quantities. The blocks of the 2×2 matrix are ss, sp, ps and pp, i.e. the 3×3 block of pp expansion coefficients is represented by a single matrix entry, etc. Specifically, the p_x valence and s conduction bands for argon are

$$\Psi_{2k}(\boldsymbol{r}) = \sum_\lambda (2\pi)^{1/2} \left(\frac{2\xi}{\pi}\right)^{5/4} (x - R_{\lambda,x}) \exp[-\xi(\boldsymbol{r} - \boldsymbol{R}_\lambda)^2] \exp[\mathrm{i}\boldsymbol{k} \cdot \boldsymbol{R}_\lambda] \tag{17a}$$

and

$$\Psi_{1k}(\boldsymbol{r}) = \sum_\lambda \left(\frac{2\xi}{\pi}\right)^{3/4} \exp[-\xi(\boldsymbol{r} - \boldsymbol{R}_\lambda)^2 \exp[\mathrm{i}\boldsymbol{k} \cdot \boldsymbol{R}_\lambda]. \tag{17b}$$

Matrix representations of v and P in the ETB basis are derived in Appendix A and, together with ε, are given by

$$\boldsymbol{v}(\boldsymbol{q}) = \frac{(2\pi)^{3/2}}{\xi^{5/2}} \frac{e^2}{4\pi\varepsilon_0} \begin{pmatrix} \left(\frac{\xi}{2\pi}\right)^{3/2} + \xi R_{1q} & \xi^{1/2} \boldsymbol{R}_{2q} \\ \xi^{1/2} \boldsymbol{R}_{2q}^* & \frac{1}{3}\left(\frac{\xi}{2\pi}\right)^{3/2} + \boldsymbol{T}_q \end{pmatrix} \tag{18}$$

$$\boldsymbol{P}(\omega) = -\frac{\xi^{5/2}}{(2\pi)^{3/2}} a\alpha(\omega) \begin{pmatrix} 0 & 0 \\ 0 & \boldsymbol{I} \end{pmatrix} \tag{19}$$

$$\varepsilon(\boldsymbol{q},\omega)=\begin{pmatrix}1 & 0\\ 0 & \boldsymbol{I}\end{pmatrix}+a\alpha(\omega)\frac{e^2}{4\pi\varepsilon_0}\left[\begin{pmatrix}0 & \xi^{1/2}\boldsymbol{R}_{2q}\\ 0 & \boldsymbol{T}_q\end{pmatrix}+\frac{1}{3}\left(\frac{\xi}{2\pi}\right)^{3/2}\begin{pmatrix}0 & 0\\ 0 & \boldsymbol{I}\end{pmatrix}\right] \tag{20}$$

where $a=8(2/3)^6=0.702\ldots$, ξ is the orbital exponent, $\alpha(\omega)=2/m((\omega_0-\mathrm{i}\delta)^2-\omega^2)$ and R_{1q}, $\boldsymbol{R}_{2q}$ are Fourier transformed lattice sums similar to $\boldsymbol{T}_q$ (appendices A and B). Diagonal terms proportional to ξ^{-1} in equation (18) are contributions to the potential energy matrix from $\boldsymbol{R}_\lambda=\boldsymbol{0}$ in equation (A.9) ('on-site' contributions) and the others are 'inter-site' contributions (from $\boldsymbol{R}_\lambda\neq\boldsymbol{0}$). ($\boldsymbol{R}_\lambda$ was previously defined to be a real space lattice vector.) $\boldsymbol{P}$ is a function of frequency only, because there is a single band gap in the ETB model and matrix elements are independent of wavevector. It contains only diagonal pp parts as matrix elements of the RPA polarizability consist of three-orbital products. The only non-zero combinations are $\langle$s|pp$\rangle$, $\langle$s|ss$\rangle$, $\langle$p|sp$\rangle$ and $\langle$p|ps$\rangle$. The RPA polarizability contains products of a p ground state and an s excited state and the only basis function to overlap with this product is an identical p orbital, which makes $\boldsymbol{P}$ diagonal.

On-site contributions to the Coulomb interaction appear in the diagonal elements of v_q; inter-site contributions can be compared to these using the fact that at small q, $R_{1q}\sim 4\pi/Vq^2$; at small q, $\boldsymbol{T}_q=8\pi/3V=8\sqrt{2\pi/3}|\boldsymbol{R}|^3$ for an fcc lattice [21] and it decreases by a factor of ~ 2 for $q\sim\pi/a$ (appendix B). ($\boldsymbol{R}$ is used to denote a primitive lattice translation vector.) Hence *inter*-site contributions dominate *on*-site contributions if $\boldsymbol{T}_q\gg 1/3(\xi/2\pi)^{3/2}$ or $\xi|\boldsymbol{R}|^2\ll 8\pi^{5/3}\sim 50$, and if $\xi\boldsymbol{R}_{1q}\gg(\xi/2\pi)^{3/2}$ or $\xi|\boldsymbol{R}|^2\ll 128\pi$ (at $q=\pi/a$ where $\boldsymbol{R}_{1q}$ is smallest). In condensed Ar the nearest neighbour separation is 3.76 Å and an appropriate value of ξ for Ar is 1.0 Å^{-2}, so that $\xi|\boldsymbol{R}|^2\sim 15$, hence the contribution from the on-site terms will be smaller than that from inter-site terms, but not insignificant. The main effect of these on-site terms in the ETB model is to shift the discrete dipole mode frequencies (which appear as plasmon pole frequencies in the model self-energy calculation) up by a small, uniform amount. A value of ξ of 1.0 Å^{-2} is equivalent to an upward shift of ~ 2 eV. The on-site term in equation (20) will be omitted from dielectric matrices from here on.

The overlap of two s Gaussian orbitals separated by a lattice constant is $\exp[-\xi|\boldsymbol{R}|^2/2]$ and so the negligible overlap criterion is satisfied provided $\xi|\boldsymbol{R}|^2\gg 2$.

In order to proceed further with this model, to calculate W and Σ, either the ETB dielectric function must be inverted numerically, or the dielectric function must be approximated so that it can be inverted otherwise. We choose to do the latter. In order to identify an approximation for the response function, R, in terms of discrete dipole eigenvectors and eigenvalues, the dielectric function in equation (20) is approximated by

$$\varepsilon(\boldsymbol{q},\omega)=\begin{pmatrix}1 & 0\\ 0 & \boldsymbol{I}+\dfrac{e^2}{4\pi\varepsilon_0}\alpha(\omega)\boldsymbol{T}_q\end{pmatrix}. \tag{21}$$

In making this approximation the off-diagonal matrix element in the first term in square brackets in equation (20) is neglected to make ε block-diagonal. Furthermore, we note that when the factor a in equation (20) is set to unity (cf $0.702\ldots$), the lower right element of the dielectric matrix in equation (21) is related to the matrix $(\alpha^{-1}+T)$ by

$$1+T\alpha=(\alpha^{-1}+T)\alpha. \tag{22}$$

$(\alpha^{-1}+T)$ is the matrix which is diagonalized to obtain discrete dipole eigenvalues and eigenvectors and its inverse can be expressed in terms of these eigenvalues and eigenvectors. The inverse of the matrix in equation (21) is therefore

$$\varepsilon^{-1}(\boldsymbol{q},\omega)=\begin{pmatrix}1 & 0\\ 0 & \alpha^{-1}(\omega)\boldsymbol{X}_q\end{pmatrix}=\begin{pmatrix}1 & 0\\ 0 & \boldsymbol{I}\end{pmatrix}-\frac{e^2}{4\pi\varepsilon_0}\begin{pmatrix}0 & 0\\ 0 & \boldsymbol{T}_q\boldsymbol{X}_q\end{pmatrix}. \tag{23}$$

The second equality in equation (23) is true because $\boldsymbol{X}_q$ is the inverse of $(\alpha^{-1} + T)$. The response function identified from equations (3), (19) and (23) is

$$R(\boldsymbol{q}, \omega) = -\frac{\xi^{5/2}}{(2\pi)^{3/2}} \begin{pmatrix} 0 & 0 \\ 0 & \boldsymbol{X}_q \end{pmatrix}. \tag{24}$$

Using this response function, the definition of ε^{-1} in equation (2) and the Coulomb interaction in equation (18), the inverse dielectric matrix is

$$\varepsilon^{-1}(\boldsymbol{q}, \omega) = \begin{pmatrix} 1 & 0 \\ 0 & \boldsymbol{I} \end{pmatrix} - \frac{e^2}{4\pi\varepsilon_0} \begin{pmatrix} 0 & \xi^{1/2}\boldsymbol{R}_{2q}\boldsymbol{X}_q \\ 0 & \boldsymbol{T}_q\boldsymbol{X}_q \end{pmatrix}. \tag{25}$$

The screened interaction (equation (4)) using equation (25) and equation (18) is

$$W(\boldsymbol{q}, \omega) = \frac{(2\pi)^{3/2}}{\xi^{5/2}} \frac{e^2}{4\pi\varepsilon_0} \times \left[\begin{pmatrix} \xi\boldsymbol{R}_{1q} & \xi^{1/2}\boldsymbol{R}_{2q} \\ \xi^{1/2}\boldsymbol{R}^*_{2q} & \boldsymbol{T}_q \end{pmatrix} - \frac{e^2}{4\pi\varepsilon_0} \begin{pmatrix} \xi\boldsymbol{R}_{2q}\boldsymbol{X}_q\boldsymbol{R}^*_{2q} & \xi^{1/2}\boldsymbol{R}_{2q}\boldsymbol{X}_q\boldsymbol{T}_q \\ \xi^{1/2}\boldsymbol{T}_q\boldsymbol{X}_q\boldsymbol{R}^*_{2q} & \boldsymbol{T}_q\boldsymbol{X}_q\boldsymbol{T}_q \end{pmatrix} \right]. \tag{26}$$

W contains the direct Coulomb interaction in the first round bracket and the screening response of the polarizable medium in the second. The ss block of the latter part describes the radial electric field coupling a virtual monopole to the surrounding dipole-polarizable medium and the induced potential at the site of the virtual monopole caused by induced dipoles. The sp block describes coupling of monopoles to the medium and the induced potential experienced by a dipole; the pp block describes coupling of dipoles to the medium and the induced potential experienced by a dipole.

Within the GW approximation, the self-energy operator is obtained from the convolution of the one-particle Green function with the screened interaction [18]

$$\Sigma(\boldsymbol{r}, \boldsymbol{r}', \omega) = \mathrm{i}\hbar \int_{-\infty}^{\infty} \frac{\mathrm{d}\omega'}{2\pi} \, \mathrm{e}^{-\mathrm{i}\delta\omega'} G_0(\boldsymbol{r}, \boldsymbol{r}', \omega - \omega') W(\boldsymbol{r}, \boldsymbol{r}', \omega') \tag{27}$$

where δ is a positive infinitesimal. The non-interacting Green function is

$$G_0(\boldsymbol{r}, \boldsymbol{r}', \omega) = 2 \sum_{i,\boldsymbol{k}} \frac{\Psi_{i\boldsymbol{k}}(\boldsymbol{r})\Psi^*_{i\boldsymbol{k}}(\boldsymbol{r}')}{\hbar(\omega - \omega_{i\boldsymbol{k}} + \mathrm{i}\delta \, \mathrm{sgn}(\varepsilon_{i\boldsymbol{k}} - \varepsilon_f)} \tag{28}$$

where the sum is over all valence and conduction band states, $\varepsilon_i = \hbar\omega_{i\boldsymbol{k}}$, is the valence band or conduction band energy and ε_f is the Fermi energy, defined to lie between the valence and conduction band states in this model. The factor of two comes from a sum over spin. If the valence band energy is denoted $\hbar\omega_v$ and the conduction band energy is denoted $\hbar\omega_c$, the matrix representation of G_0 in the Gaussian orbital basis is

$$G_0(\boldsymbol{k}, \omega) = \frac{2}{\hbar} \begin{pmatrix} \dfrac{1}{\omega - \omega_c + \mathrm{i}\delta} & 0 \\ 0 & \dfrac{1}{\omega - \omega_v - \mathrm{i}\delta} \boldsymbol{I} \end{pmatrix}. \tag{29}$$

Evaluation of the self-energy for a particular state involves a contour integration (equation (7)) along the real axis in the upper-half complex plane and spatial integrals in two spatial variables, $\boldsymbol{r}$ and $\boldsymbol{r}'$. Each spatial integral involves the state itself and one basis function from each of W and the intermediate G_0 in the rightmost diagram in figure 1. The spatial integrals determine the multipolar nature of the screening. Scattering into the intermediate states in this G_0 produces a virtual monopole or dipole depending on whether the scattering event is an intra- or inter-band scattering. Matrix elements of the self-energy operator are given in equation (30) and (31) (note that these are not coefficients of a matrix expansion

of the self-energy operator). Equation (30) gives contributions to the self-energy from the unscreened Coulomb interaction and divides this into on-site and inter-site parts; this is the static Hartree–Fock exchange [19].

$$\Sigma_{HF}^{on\text{-}site} = -\frac{2^9}{3^5}\frac{e^2}{4\pi\varepsilon_0}\begin{pmatrix} 0 & 0 \\ 0 & \dfrac{\xi^{1/2}}{3(2\pi)^{3/2}} \end{pmatrix} \tag{30a}$$

$$\Sigma_{q_{HF}}^{inter\text{-}site} = -\frac{2^9}{3^5}\frac{e^2}{4\pi\varepsilon_0}\begin{pmatrix} \dfrac{1}{\xi}\operatorname{Tr}\boldsymbol{T}_q & \xi^{-1/2}\boldsymbol{R}_{2q}^* \\ \xi^{-1/2}\boldsymbol{R}_{2q} & \boldsymbol{R}_{1q}\boldsymbol{I} \end{pmatrix}. \tag{30b}$$

Equation (31) gives the contribution to the self-energy from the dynamic part of W [1], i.e. the Coulomb hole and screened exchange contributions [18, 19],

$$\begin{aligned}\Sigma(\boldsymbol{q},\omega) = \frac{1}{2\Omega_{nq}}\frac{1}{(\omega-\omega_i+\operatorname{sgn}(\varepsilon_f-\hbar\omega_i)\Omega_{nq})}\frac{2^9}{3^5}\left(\frac{e^2}{4\pi\varepsilon_0}\right)^2 \\ \times\left[\frac{1}{4}\begin{pmatrix} \boldsymbol{R}_{2q}\boldsymbol{X}_q\boldsymbol{R}_{2q}^* & \xi^{-1/2}\boldsymbol{R}_{2q}^*\boldsymbol{X}_q\boldsymbol{T}_q \\ \xi^{-1/2}\boldsymbol{T}_q\boldsymbol{X}_q\boldsymbol{R}_{2q}^* & \dfrac{1}{\xi}\boldsymbol{T}_q\boldsymbol{X}_q\boldsymbol{T}_q \end{pmatrix}_{i=1}\right. \\ \left.+\begin{pmatrix} \dfrac{1}{\xi}\operatorname{Tr}\boldsymbol{T}_q\boldsymbol{X}_q\boldsymbol{T}_q & \xi^{-1/2}(\boldsymbol{T}_q\boldsymbol{X}_q\boldsymbol{R}_{1q}^*)^{\boldsymbol{T}} \\ \xi^{-1/2}(\boldsymbol{R}_{2q}^*\boldsymbol{X}_q\boldsymbol{T}_q)^{\boldsymbol{T}} & \boldsymbol{R}_{2q}\boldsymbol{X}_q\boldsymbol{R}_{2q}^*\boldsymbol{I} \end{pmatrix}_{i=2-4}\right].\end{aligned} \tag{31}$$

The subscript i in equation (31) refers to the self-energy when the intermediate state is a conduction band state ($i = 1$) and when the intermediate state is a valence band state ($i = 2$–4). Note that the frequency denominators have been integrated out of the response function $\boldsymbol{X}_q$ in equation (31). Hence the diagonal matrix element of the self-energy operator for conduction band states contains the terms $\boldsymbol{R}_{2q}\boldsymbol{X}_q\boldsymbol{R}_{2q}^*$ and $\operatorname{Tr}\boldsymbol{T}_q\boldsymbol{X}_q\boldsymbol{T}_q$. The first term arises from intra-band scattering and the latter from inter-band scattering. The trace in the latter term arises as there are several p states available as intermediate states. The diagonal matrix element of the self-energy operator for valence band states contains the terms $\boldsymbol{R}_{2q}\boldsymbol{X}_q\boldsymbol{R}_{2q}^*$ and $\boldsymbol{T}_q\boldsymbol{X}_q\boldsymbol{T}_q$. There is no trace in the second term as there is only one intermediate conduction band in the ETB model.

3. Dispersion relations and self-energies

In this section plasmon pole dispersion relations are presented for Ar calculated from the discrete dipole equations (equation (12) and (13)) and these are used to calculate matrix elements of the self-energy operator for the ETB valence and conduction band states using equation (31). The plasmon pole energies, Ω_q, appear in the frequency denominator in equation (31) and the discrete dipole eigenvectors appear in the response function, $\boldsymbol{X}_q$. Self-energy matrix elements are compared to *ab initio* calculations of matrix elements of valence and conduction band states in the bulk solid.

The plasmon pole dispersion relation obtained by solving equation (12) and (13), for Ar along the Λ and Δ directions in the Brillouin zone is shown in figure 2. A static Ar polarizability of 1.20×10^{-40} C m^2 V^{-1} located at atom centres, an effective mass of 1.0, in units of the bare electron mass, and a nearest neighbour distance of 3.76 Å were used. The polarizability and effective mass used result in a Γ point transverse mode energy of $\hbar(\omega_c - \omega_v) = 14.3$ eV, equivalent to the electron–hole energy gap (excluding excitonic effects) in solid Ar [22]. This value is less than the experimental value for the static

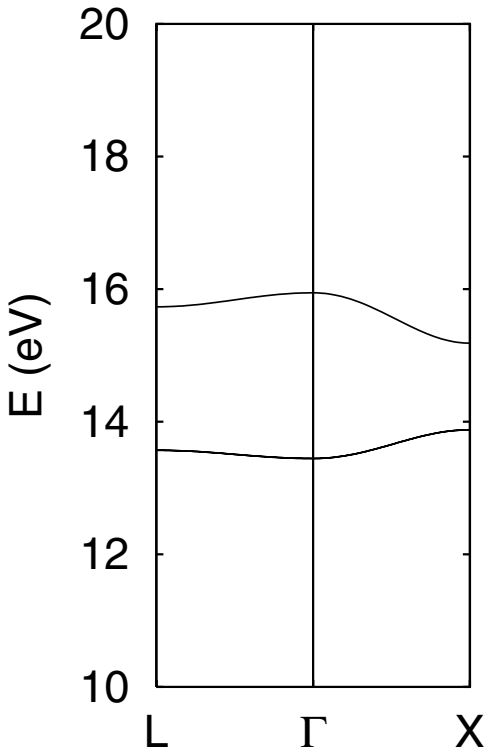

Figure 2. Plasmon energy versus wavevector for fcc argon with isotropic polarizability of 1.20×10^{-40} C m^2 V^{-1}. The upper mode is longitudinal and the lower modes are a degenerate pair of transverse modes.

polarizability of argon derived from the macroscopic dielectric function and the Claussius–Mossotti function [22], 1.83×10^{-40} C m^2 V^{-1}. The dispersion relation contains a longitudinal (L) branch and two degenerate transverse (T) branches of lower energy. The L–T splitting is relatively small owing to the low polarizability density of Ar.

The energy-dependent parts of the self-energy for Ar valence and conduction band states (i.e. the self-energy excluding the static Hartree–Fock part as in equation (30)), are shown in figures 3 and 4. These figures show the self-energy calculated using the ETB model and an *ab initio* code with input wavefunctions and energy eigenvalues from a local density approximation–density functional (LDA–DF) band structure calculation performed using a Gaussian orbital basis [23]. The *ab initio* self-energy curves were obtained for valence and conduction band states at the Γ point of the Brillouin zone. The valence band energy for the ETB model and valence band maximum for the *ab initio* calculation were chosen to be at zero energy. The LDA–DF band gap was 13.6 eV.

The ETB model self-energy for a p valence band state is given by the terms on the bottom right in the square brackets in equation (31). The term containing the factor $\boldsymbol{R}_{2q}\boldsymbol{X}_q\boldsymbol{R}_{2q}^*$ arises from intra-band scattering while the term containing the factor $\boldsymbol{T}_q\boldsymbol{X}_q\boldsymbol{T}_q$ arises from inter-band scattering. As noted above, the former scattering process results in induction of virtual monopoles on lattice sites while the latter results in induction of virtual dipoles. Intra-band scattering for the p valence state results in a peak in the self-energy curve around -16 eV (figure 3) while inter-band scattering results in a very weak peak around +30 eV (figure 3).

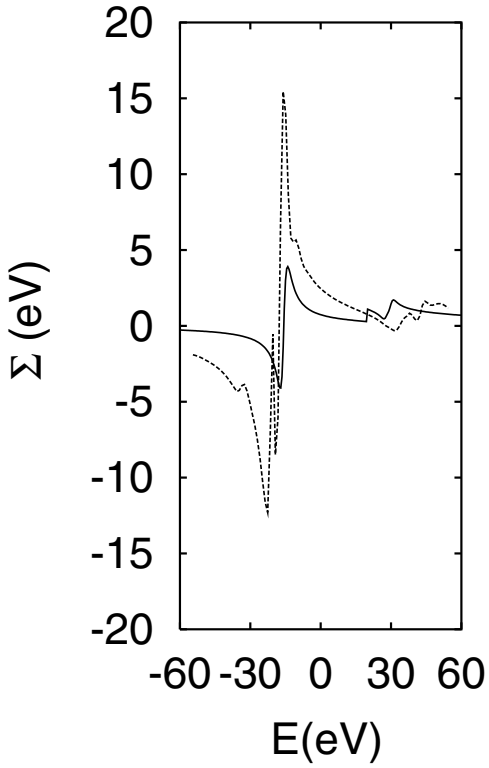

Figure 3. Energy dependence of valence band matrix elements of the self-energy operator of fcc argon. ETB model (solid line), *ab initio* calculation for a valence band state at the Γ point of the Brillouin zone (dashed line). The ETB self-energy curve has been scaled by a factor of 4 above 20 eV.

The *ab initio* self-energy calculation shows several intra-band scattering peaks for valence states around −25 eV, which are several times larger than that of the ETB model. The *ab initio* calculation shows that the inter-band scattering contributes much smaller peaks (∼2 eV peak to peak height around +30 eV) than intra-band scattering for either valence or conduction band states.

The ETB model self-energy for an s conduction band state is given by the terms on the upper left in square brackets in equation (31). The terms containing the factors $\boldsymbol{R}_{2q}\boldsymbol{X}_q\boldsymbol{R}^*_{2q}$ and $\boldsymbol{T}_q\boldsymbol{X}_q\boldsymbol{T}_q$ again arise from intra- and inter-band scattering events. Intra-band scattering for the s state in the ETB model results in a peak around +30 eV while inter-band scattering results in a peak around −16 eV. In this case the ETB and *ab initio* calculations disagree on the magnitude of the intra- and inter-band scattering.

4. Discussion

In previous sections we presented a model and *ab initio* calculations for the self-energy of valence and conduction band electrons in a solid with a simple electronic structure, solid Ar. In this section we discuss the ETB model in the light of the results of *ab initio* calculations on Ar. We also make several observations regarding screening in Ar and compare screening in Ar in the ETB model to Clausius–Mossotti screening. We consider how virtual monopoles

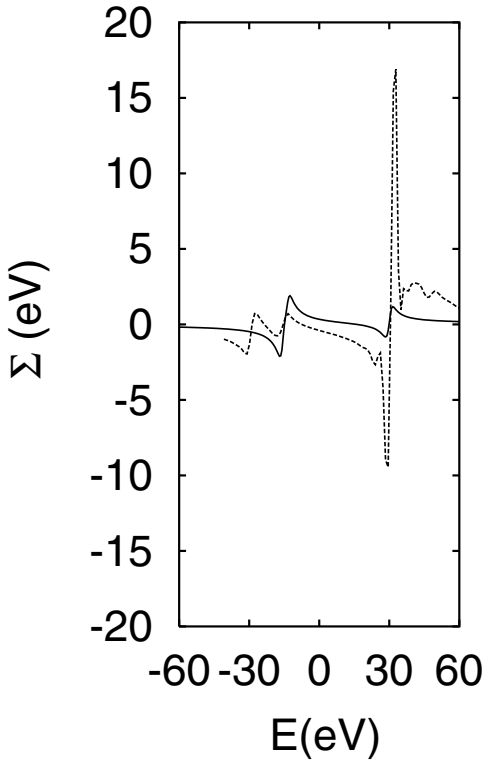

Figure 4. Energy dependence of conduction band matrix elements of the self-energy operator of fcc argon. ETB model (solid line), *ab initio* calculation for the lowest energy conduction band state at the Γ point of the Brillouin zone (dashed line).

and dipoles couple to the screening dipoles and how effectively these screen monopoles and dipoles.

The model presented above is transparent but fails to give a quantitative account of the energy dependence of the self-energy in Ar; plasmon energies tend to be too low and there is structure in the *ab initio* self-energy curves which cannot be explained using the model. This may be due to the severe approximations regarding magnitudes of matrix elements in the model. However, we believe that it is more likely that this is because of omission of important terms in the polarizability (equation (19)). The only part of the polarizability included in this model is the dipole–dipole part; monopole–monopole terms and others have been omitted. The monopolar term in the polarizability would arise, for example, from valence band 3p and conduction band 4p derived states and would appear in the top right element of the matrix representing the polarizability (equation (19)). 4p derived bands lie 30.5 eV above the valence band maximum in our LDA–DF calculation. Interaction between dipolar and monopolar transitions could produce the structure in the *ab initio* self-energy curves (figures 3 and 4). Evidence for the importance of these modes is provided by the dielectric band structure [24] of Ar [23], where it is found that the eigenvalue of the Hermitian, inverse dielectric function with the *smallest* value (in a sense, the most screening) corresponds to an eigenpotential which is spherically symmetric about each atom centre.

Polarization associated with a spherically symmetric eigenpotential is shrinking or expansion of the atomic charge sphere. This will obviously be important in the self-energy of

electrons or holes in the solid. On the other hand, this type of polarization process does not directly determine the optical properties of the material. Instead these are directly determined by transverse dipolar polarization. Hence, the discrete dipole model is successful in describing optical properties of semiconductors but a more general multipolar model of polarization is necessary to describe both optical properties and the self-energies of materials. Inclusion of both the monopolar and dipolar parts of the polarizability in equation (19) would lead to a problem requiring numerical inversion of the dielectric function and is beyond the scope of the present paper.

We continue with a discussion of screening of virtual monopoles and dipoles by the dipolar part of the response function. For a centrosymmetric crystal structure such as the fcc structure, the lattice sums R_{1q}, $\boldsymbol{R}_{2q}$ and $\boldsymbol{T}_q$ are pure real, imaginary and complex, respectively. Screening of a virtual 's monopole' is proportional to $\boldsymbol{R}_{2q}\boldsymbol{X}_q\boldsymbol{R}^*_{2q}$. Since $\boldsymbol{R}_{2q}$ is pure imaginary, this term is negative and counteracts the direct Coulomb interaction, R_{1q}, with other charges in the system, as expected in a screened interaction. The vector lattice sum $\boldsymbol{R}_{2q}$ also has the property that it is parallel to the wavevector, $\boldsymbol{q}$. This ensures that only dipole waves with a longitudinal component couple to the monopole and screen it. Here *longitudinal component* means that the dipole wave eigenvector has a non-zero component parallel to the wavevector, $\boldsymbol{q}$.

Screening of virtual monopoles and dipoles in Ar is qualitatively different. The term $\boldsymbol{T}_q\boldsymbol{X}_q\boldsymbol{T}_q$ in the self-energy in equation (31) is due to inter-band scattering, which leads to formation of virtual dipoles on lattice sites, which can excite *both* L and T polarization waves. The fact that transverse polarization waves can contribute to screening of electrons and holes is somewhat surprising since point charges generate purely longitudinal fields. However, scattering of an electron or hole from a state s_k to a state p_{k+q} leads to a longitudinal (transverse) polarization wave if the axis of the p orbital is parallel (perpendicular) to the wavevector, $\boldsymbol{q}$, and the transverse polarization wave can couple to T modes in the response function. We consider the particular case of contributions of L and T modes to the term $\boldsymbol{T}_q\boldsymbol{X}_q\boldsymbol{T}_q$ in the self-energy. For a small wavevector $\boldsymbol{q} \parallel \boldsymbol{x}$, $\boldsymbol{T}_q$ is proportional to

$$\begin{pmatrix} 2 & 0 & 0 \\ 0 & -1 & 0 \\ 0 & 0 & -1 \end{pmatrix}. \tag{32}$$

The eigenvectors which make up $\boldsymbol{X}_q$ are directed along x (L mode), y or z (T modes) and so the matrix $\boldsymbol{T}_q\boldsymbol{X}_q\boldsymbol{T}_q$ contributing to the self-energy is proportional to

$$\begin{pmatrix} 4 & 0 & 0 \\ 0 & 2 & 0 \\ 0 & 0 & 2 \end{pmatrix} \tag{33}$$

the first entry on the diagonal in equation (33) arises from the L mode polarized $\parallel \boldsymbol{x}$ and the second two from the T modes polarized $\parallel \boldsymbol{y}$ or $\boldsymbol{z}$.

In a model for screening involving interacting point dipoles it is reasonable to expect that the dielectric function for screening at long range (small wavevector, $\boldsymbol{q}$) will be the Clausius–Mossotti dielectric function, ε. We now demonstrate that the inverse dielectric function for screening of the field due to a monopole in the ETB model is that given by the Clausius–Mossotti dielectric function. The Clausius–Mossotti (CM) relation between the polarizability, α, and macroscopic dielectric function, ε, is

$$\frac{\varepsilon - 1}{\varepsilon + 2} = \frac{\alpha}{3\varepsilon_0 V}. \tag{34}$$

The static, inverse dielectric constant, $1/\varepsilon$, is then expressed as $1 - A$, where

$$A = \frac{\alpha/\varepsilon_0 V}{1 + 2\alpha/3\varepsilon_0 V}. \tag{35}$$

A may be rewritten as

$$A = \frac{e^2}{4\pi\varepsilon_0}\frac{8\pi}{V}\frac{1}{m\Omega_q^2} \tag{36}$$

by noting that for a monatomic lattice $\boldsymbol{T_q}$ is diagonal and has elements $V\boldsymbol{T_q} = (4\pi/3)(2,-1,-1)$ in the long wavelength limit [21]. Replacing the longitudinal part of $\boldsymbol{T_q}$ by $8\pi/3V$ in equation (11),

$$\left(\alpha^{-1} + \frac{T_q}{4\pi\varepsilon_0}\right) = \frac{m\Omega_q^2}{2e^2} \tag{37}$$

and using this relation in equation (35) gives the result in equation (36).

At small wavevector $R_{1q} \sim 4\pi/Vq^2$ and $\boldsymbol{R}_{2q} \sim 4\pi/Vq$ (appendix B). Using these approximations and equations (15) and (26), the ss block of the screened interaction at long wavelength is approximately

$$W_{qss} = \left(\frac{2\pi}{\xi}\right)^{3/2}\frac{e^2}{4\pi\varepsilon_0}\frac{4\pi}{Vq^2}\left(1 - \frac{e^2}{4\pi\varepsilon_0}\frac{8\pi}{V}\frac{1}{m\Omega_q^2}\right). \tag{38}$$

Since, at long wavelength, the second term in brackets is A, W_{qss} is the Coulomb potential screened to the extent given by CM.

5. Conclusion

The discrete dipole model is generally regarded as a phenomenological model for optical properties of semiconductors. We have shown that the dielectric function of an insulator can be expressed in terms of discrete dipole eigenvectors and dipole wave energies in an extreme tight binding model. The ETB model has been used to obtain an expression for the screened interactions and self-energies of electron and hole states in Ar in terms of lattice sums. When self-energies for these states calculated using the ETB model are compared to self-energies obtained in an *ab initio* calculation, it is found that structure in the *ab initio* calculations and relative magnitudes of peaks in the self-energy curves are not reproduced by the model. The discrete dipole polarizability and response functions contain only dipolar polarization processes; these are obviously important in determining optical properties of semiconductors but important monopolar polarization processes are omitted in the present model and are expected to be important in determining electron and hole self-energies.

Acknowledgments

This work was supported by Enterprise Ireland under grant number 99/SC/255. MN wishes to thank the Trinity Foundation for a Research Fellowship. The self-energy code used for this work was written by M Kuzmin.

Appendix A. The ETB dielectric matrix

The RPA polarizability (equation (1)) is given by equation (73) in [19],

$$P(\boldsymbol{r},\boldsymbol{r}',\omega) = 2\sum_{ik}^{occ}\sum_{jk'}^{unocc}\Psi_{ik}^*(\boldsymbol{r})\Psi_{jk'}\Psi_{jk'}^*(\boldsymbol{r}')\Psi_{ik}(\boldsymbol{r}') \times\left[\frac{1}{\omega - E_{jk'} + E_{ik} + \mathrm{i}\delta} - \frac{1}{\omega + E_{jk'} - E_{ik} - \mathrm{i}\delta}\right]. \tag{A.1}$$

The numerator in equation (A.1) consists of products of valence band and conduction band states at different $\boldsymbol{k}$ points. Owing to lattice translation symmetry, the polarizability function has the periodicity of the lattice, i.e. $P(\boldsymbol{r}+\boldsymbol{R},\boldsymbol{r}'+\boldsymbol{R}) = P(\boldsymbol{r},\boldsymbol{r}')$, where $\boldsymbol{R}$ is any lattice translation vector, and may therefore be expanded in an orbital basis such as that in equation (74) in [19] as

$$P(\boldsymbol{r},\boldsymbol{r}',\omega) = \sum_{ijq} P_{ij}(\boldsymbol{q},\omega)\Psi_{iq}(\boldsymbol{r})\Psi^*_{jq}(\boldsymbol{r}'). \tag{A.2}$$

The expansion is limited to the same set of s and p Gaussian functions as used for the valence and conduction bands. Since the expansion functions and wavefunctions are independent of wavevector in the ETB approximation, the $\boldsymbol{k}$ or $\boldsymbol{q}$ index on these functions is omitted in the remainder of this appendix. Coefficients in the expansion are determined from a double integration over the unit cell volume, V [19],

$$P_{ij}(\boldsymbol{q},\omega) = \int\int_V \mathrm{d}\boldsymbol{r}\,\mathrm{d}^3\boldsymbol{r}'\Psi^*_i(\boldsymbol{r})P(\boldsymbol{r},\boldsymbol{r}',\omega)\Psi^*_j(\boldsymbol{r}'). \tag{A.3}$$

Matrix elements in equation (A.3) are non-zero *only* when both expansion orbitals (Ψ_i, Ψ_j) are identical p orbitals when the wavefunctions satisfy the non-overlapping condition assumed in the ETB model. The non-zero matrix elements obtained by substituting P from equation (A.1) into equation (A.3) are

$$|\langle\Psi_p \mid \Psi_s\Psi_p\rangle|^2 = \left(\frac{\xi}{2\pi}\right)^{3/2} 2^8 3^{-5} \tag{A.4a}$$

$$|\langle\Psi_s \mid \Psi_s\Psi_s\rangle|^2 = \left(\frac{\xi}{2\pi}\right)^{3/2} 2^6 3^{-3}. \tag{A.4b}$$

Since there is only one optical transition energy, $E_g = E_{k'} - E_k = \hbar\omega_0$, the denominators in equation (A.1) may be rewritten as

$$\sum_q \frac{-4E_g}{(E_g - \mathrm{i}\delta)^2 - \omega^2}. \tag{A.5}$$

The oscillator strength sum rule may be used to deduce a value for E_g in terms of ξ. There are six transitions per electron pair in the ETB model and the oscillator strength sum rule [25] requires that

$$\frac{2m\hbar\omega_0}{\hbar^2}|\langle\Psi_{1q}|x|\Psi_{2q}\rangle|^2 = \frac{1}{6}. \tag{A.6}$$

The squared dipole matrix element in equation (A.6) is equal to $1/4\xi$. Equations (A.3) to (A.6) can therefore be used to express the polarizability for one site per primitive cell as

$$\boldsymbol{P}(\omega) = -\frac{\xi^{5/2}}{(2\pi)^{3/2}}\frac{2^9}{3^6}\frac{2}{(\omega_0 - \mathrm{i}\delta)^2 - \omega^2}\begin{pmatrix}0 & 0\\ 0 & \boldsymbol{I}\end{pmatrix} = -\frac{\xi^{5/2}}{(2\pi)^{3/2}}a\alpha(\omega)\begin{pmatrix}0 & 0\\ 0 & \boldsymbol{I}\end{pmatrix} \tag{A.7}$$

where $a = 8(2/3)^6$ and $\alpha(\omega) = 2/m((\omega_0 - \mathrm{i}\delta)^2 - \omega^2)$.

The Coulomb potential may be expanded similarly as

$$\frac{e^2}{|\boldsymbol{r}-\boldsymbol{r}'|} = \sum_{ijq} v_{ij}(\boldsymbol{q})\Psi_i(\boldsymbol{r})\Psi^*_j(\boldsymbol{r}') \tag{A.8}$$

with expansion coefficients given by

$$v_{ij}(\boldsymbol{q}) = \sum_\lambda \int\int_V \mathrm{d}^3\boldsymbol{r}\,\mathrm{d}^3\boldsymbol{r}'\frac{\Psi^*_i(\boldsymbol{r})\exp[\mathrm{i}\boldsymbol{q}\cdot\boldsymbol{R}_\lambda]\Psi_j(\boldsymbol{r}')}{|\boldsymbol{R}_\lambda + \boldsymbol{r}' - \boldsymbol{r}|}. \tag{A.9}$$

In order to demonstrate the equivalence of the discrete dipole and ETB models, a Taylor expansion of the denominator of equation (A.9) is made,

$$\frac{1}{|\boldsymbol{R}+\boldsymbol{r}'-\boldsymbol{r}|}=\frac{1}{\boldsymbol{R}}-\frac{(\boldsymbol{r}'-\boldsymbol{r})\cdot\boldsymbol{R}}{|\boldsymbol{R}|^3}+\frac{(\boldsymbol{r}'-\boldsymbol{r})(\boldsymbol{r}'-\boldsymbol{r})}{2!}:\frac{3\boldsymbol{R}\boldsymbol{R}^T-\boldsymbol{R}^2\boldsymbol{I}}{|\boldsymbol{R}|^5}+\cdots. \tag{A.10}$$

The third term on the right-hand side of equation (A.10) contains the dipole–dipole interaction tensor,

$$\boldsymbol{t}=-\frac{3\boldsymbol{R}\boldsymbol{R}^T-|\boldsymbol{R}|^2\boldsymbol{I}}{|\boldsymbol{R}|^5}. \tag{A.11}$$

The expansion coefficients of the Coulomb potential contain lattice sums of integrals (equation (A.9)) over the local coordinates $\boldsymbol{r}$ and $\boldsymbol{r}'$, multiplied by the factor $\exp[\mathrm{i}\boldsymbol{q}\cdot\boldsymbol{R}_\lambda]$. The leading term in the expansion depends on the particular Gaussian expansion functions. When both functions are s orbitals, the leading term is proportional to $1/|\boldsymbol{R}|$, for one s orbital and one p orbital, the leading term is proportional to $\boldsymbol{R}/|\boldsymbol{R}|^3$, for both p orbitals the expansion coefficients are the dipole–dipole interaction tensors which appear in the discrete dipole model. The top right elements of the symmetric, Coulomb potential matrix, omitting a common factor of $\sum_\lambda \exp[\mathrm{i}\boldsymbol{q}\cdot\boldsymbol{R}_\lambda]$, are

$$\begin{pmatrix} \dfrac{1}{\xi}+\left(\dfrac{2\pi}{\xi}\right)^{3/2}\dfrac{1}{|\boldsymbol{R}_\lambda|} & \dfrac{(2\pi)^{3/2}}{\xi^2}\dfrac{R_x}{|\boldsymbol{R}_\lambda|^3} & \dfrac{(2\pi)^{3/2}}{\xi^2}\dfrac{R_y}{|\boldsymbol{R}_\lambda|^3} & \dfrac{(2\pi)^{3/2}}{\xi^2}\dfrac{R_z}{|\boldsymbol{R}_\lambda|^3} \\ & \dfrac{1}{3\xi}+\dfrac{(2\pi)^{3/2}}{\xi^{5/2}}T_{xx} & \dfrac{(2\pi)^{3/2}}{\xi^{5/2}}T_{xy} & \dfrac{(2\pi)^{3/2}}{\xi^{5/2}}T_{xz} \\ & & \dfrac{1}{3\xi}+\dfrac{(2\pi)^{3/2}}{\xi^{5/2}}T_{yy} & \dfrac{(2\pi)^{3/2}}{\xi^{5/2}}T_{yz} \\ & & & \dfrac{1}{3\xi}+\dfrac{(2\pi)^{3/2}}{\xi^{5/2}}T_{zz} \end{pmatrix}. \tag{A.12}$$

The matrix consists of a 1×1 ss block on the top left, a 3×3 pp block on the bottom left and 1×3 and 3×1 sp and ps blocks. The diagonal elements $1/\xi$ and $1/3\xi$ come from terms in equation (A.9) where $\boldsymbol{R}_\lambda=\boldsymbol{0}$. Equivalent self-interaction or 'on-site' terms are omitted in discrete dipole lattice sums.

Appendix B. Lattice sums

The Ewald lattice sum for the ss block of the potential matrix (equation (A.12)) is

$$R_{1q}(\boldsymbol{A})=\sum_\lambda{}' \frac{\mathrm{e}^{\mathrm{i}\boldsymbol{q}\cdot\boldsymbol{R}_\lambda}}{|\boldsymbol{R}_\lambda-\boldsymbol{A}|}. \tag{B.1}$$

$\boldsymbol{A}$ is the field point for the lattice sum with sources distributed with strength $\exp[\mathrm{i}\boldsymbol{q}\cdot\boldsymbol{R}_\lambda]$ on the lattice, $\boldsymbol{R}_\lambda$ is a lattice translation vector and the sum is over the entire infinite lattice with the exception of $\boldsymbol{R}_\lambda=\boldsymbol{0}$. For the fcc lattice the only sum required is the sum with $\boldsymbol{A}=\boldsymbol{0}$. This sum may be uniquely evaluated using the technique described by Nijboer and de Wette [26] using the expression

$$R_{1q}(\boldsymbol{A})=\left[\sum_\lambda{}' \frac{\Gamma(1/2,\pi|\boldsymbol{R}_\lambda-\boldsymbol{A}|^2)\,\mathrm{e}^{\mathrm{i}\boldsymbol{q}\cdot\boldsymbol{R}_\lambda}}{\sqrt{\pi}|\boldsymbol{R}_\lambda-\boldsymbol{A}|}-\frac{\gamma(1/2,\pi|\boldsymbol{A}|^2)}{\sqrt{\pi}|\boldsymbol{A}|}\right.$$
$$\left.+\frac{4\pi^{3/2}}{V}\sum_\lambda \frac{\Gamma(1,|\boldsymbol{G}_\lambda-\boldsymbol{q}|^2/4\pi)\,\mathrm{e}^{\mathrm{i}(\boldsymbol{G}_\lambda-\boldsymbol{q})\cdot\boldsymbol{A}}}{|\boldsymbol{G}_\lambda-\boldsymbol{q}|^2}\right]. \tag{B.2}$$

Γ and γ are the incomplete gamma function and complementary incomplete gamma functions, respectively. The second term on the right-hand side of equation (B.2) has a limiting value

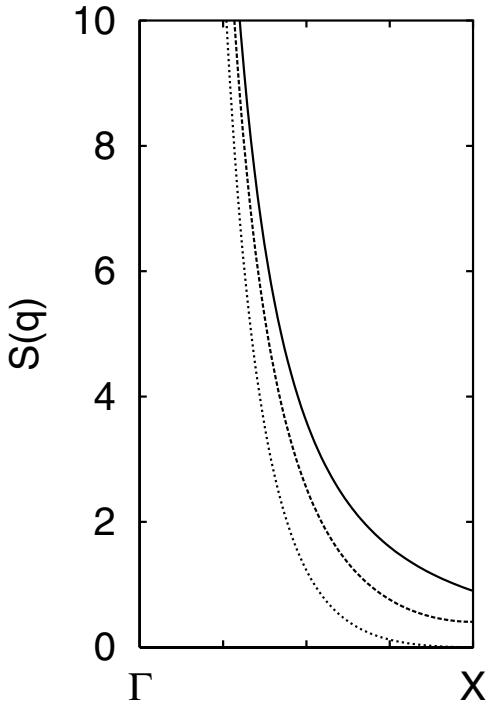

Figure B1. Dependence of R_{1q} (dotted line) and $|\boldsymbol{R}_{2q}|^2$ (dashed line) lattice sums on $\boldsymbol{q}$ in an fcc lattice for $\boldsymbol{q}$ from Γ to X. A constant of 2 has been added in R_{1q} corresponding to the $\boldsymbol{R}_\lambda = \boldsymbol{0}$ term in that sum. The fcc nearest neighbour distance has been chosen as the unit of length. The function $4\pi/Vq^2$ is shown for comparison (solid line) as the sums tend to this function at small q. The generic label $S(q)$ is used for the magnitude of each lattice sum.

of $-2\sqrt{\pi}$ as $\boldsymbol{A}$ tends to the null vector. $\boldsymbol{G}_\lambda$ is a reciprocal lattice vector and the sum is over the entire reciprocal lattice. The lattice sums required for the sp and ps blocks of the potential matrix are obtained from

$$\partial_{\boldsymbol{A}} R_{1q}(\boldsymbol{A}) = \boldsymbol{R}_{2q}(\boldsymbol{A}) = \sum_\lambda \frac{(\boldsymbol{R}_\lambda - \boldsymbol{A})\,\mathrm{e}^{\mathrm{i}\boldsymbol{q}\cdot\boldsymbol{R}_\lambda}}{|\boldsymbol{R}_\lambda - \boldsymbol{A}|^3} \tag{B.3}$$

by differentiating the expression in equation (B.2). The result is

$$\begin{aligned}\boldsymbol{R}_{2q} = \sum_\lambda \frac{(\boldsymbol{R}_\lambda - \boldsymbol{A})\,\mathrm{e}^{\mathrm{i}\boldsymbol{q}\cdot\boldsymbol{R}_\lambda}}{|\boldsymbol{R}_\lambda - \boldsymbol{A}|^2}\left[\frac{\Gamma(1/2, \pi|\boldsymbol{R}_\lambda - \boldsymbol{A}|^2)}{\sqrt{\pi}|\boldsymbol{R}_\lambda - \boldsymbol{A}|} + 2\,\mathrm{e}^{-\pi|\boldsymbol{R}_\lambda - \boldsymbol{A}|^2}\right] \\ + \frac{\boldsymbol{A}}{|\boldsymbol{A}|^2}\left[\frac{\gamma(1/2, \pi|\boldsymbol{A}|^2)}{\sqrt{\pi}|\boldsymbol{A}|} - 2\,\mathrm{e}^{-\pi|\boldsymbol{R}_\lambda - \boldsymbol{A}|^2}\right] \\ + \frac{4\pi^{3/2}\mathrm{i}}{V}\sum_\lambda (\boldsymbol{G}_\lambda - \boldsymbol{q})\frac{\Gamma(1, |\boldsymbol{G}_\lambda - \boldsymbol{q}|^2/4\pi)\,\mathrm{e}^{\mathrm{i}(\boldsymbol{G}_\lambda - \boldsymbol{q})\cdot\boldsymbol{A}}}{|\boldsymbol{G}_\lambda - \boldsymbol{q}|^2}.\end{aligned} \tag{B.4}$$

The second term in square brackets in equation (B.4) goes to zero linearly as $\boldsymbol{A}$ tends to $\boldsymbol{0}$. R_{1q} and $\boldsymbol{R}_{2q}$ sums for an fcc lattice with $\boldsymbol{A} = \boldsymbol{0}$ and wavevector ranging from the Γ to the X point of the Brillouin zone are shown in figure B1. At small wavevector R_{1q} and $\boldsymbol{R}_{2q}$ are dominated by reciprocal lattice sums; R_{1q} behaves like $4\pi/Vq^2$ and $\boldsymbol{R}_{2q}$ behaves like $4\pi/Vq$ at small q, which is to be expected as these are the discrete Fourier transforms of $1/r$ and $\boldsymbol{r}/r^3$.

Lattice sums required for the pp block of the Coulomb potential are obtained from

$$\partial_{\boldsymbol{A}} \boldsymbol{R}_{2q}(\boldsymbol{A}) = -\boldsymbol{T}_{\boldsymbol{q}}(\boldsymbol{A}) = \sum_{\lambda} \frac{3(\boldsymbol{R}_\lambda - \boldsymbol{A})(\boldsymbol{R}_\lambda - \boldsymbol{A})^{\boldsymbol{T}} - |(\boldsymbol{R}_\lambda - \boldsymbol{A})|^2 \boldsymbol{I}}{|\boldsymbol{R}_\lambda - \boldsymbol{A}|^5} \, \mathrm{e}^{\mathrm{i}\boldsymbol{q}\cdot\boldsymbol{R}_\lambda}. \tag{B.5}$$

These were evaluated using a method described by Born and Huang in equation (30.30) and equation (30.31) in [27]. These lattice sums are weakly dependent on $\boldsymbol{q}$.

References

[1] Hybertsen M S and Louie S G 1986 *Phys. Rev.* B **34** 5390
von der Linden W and Horsch P 1988 *Phys. Rev.* B **37** 8351
Hott R 1991 *Phys. Rev.* B **44** 1057
Rohlfing M, Krüger P and Pollmann J 1995 *Phys. Rev.* B **52** 1905

[2] Ewald P P 1916 *Ann. Phys.* **49** 117
Ewald P P 1917 *Ann. Phys.* **54** 519
Ewald P P 1917 *Ann. Phys.* **54** 557

[3] Herrendörfer D and Patterson C H 1997 *J. Phys. Chem. Solids* **58** 207

[4] Mahan G D and Obermair G 1969 *Phys. Rev.* **183** 834

[5] Litzman O and Rosza P 1977 *Surf. Sci.* **66** 542

[6] Grindlay J 1980 *Physica* A **107** 471

[7] Wijers C M J, Del Sole R and Manghi F 1991 *Phys. Rev.* B **44** 1825
Wijers C M J and Poppe G P M 1992 *Phys. Rev.* B **46** 7605

[8] Schaich W L and Mendoza B S 1992 *Phys. Rev.* B **45** 14 279

[9] Mochan W L and Barrera R G 1985 *Phys. Rev. Lett.* **44** 1192
Mendoza B S and Mochan W L 1996 *Phys. Rev.* B **53** R10 473

[10] Herrendörfer D and Patterson C H 1997 *Surf. Sci.* **375** 210
Hogan C D and Patterson C H 1998 *Phys. Rev.* B **57** 14 843

[11] Purcell E M and Pennypacker C R 1973 *Astrophys. J.* **186** 705
Draine B T 1988 *Astrophys. J.* **333** 848

[12] Penn D R 1962 *Phys. Rev.* **128** 2093

[13] Sinha S K 1969 *Phys. Rev.* **177** 1256
Sinha S K, Gupta R P and Price D L 1974 *Phys. Rev.* B **9** 2564
Sinha S K, Gupta R P and Price D L 1974 *Phys. Rev.* B **9** 2573

[14] Johnson D L 1974 *Phys. Rev.* B **9** 4475

[15] Ortuno M and Inkson J C 1979 *J. Phys. C: Solid State Phys.* **12** 1065
Sterne P A and Inkson J C 1984 *J. Phys. C: Solid State Phys.* **17** 1497
Inkson J C and Sharma A C 1985 *J. Phys. C: Solid State Phys.* **18** 5435
Ortuno M and Inkson J C 1985 *Solid State Commun.* **55** 367

[16] Car R and Selloni A 1979 *Phys. Rev. Lett.* **40** 1365

[17] Toyozawa Y 1954 *Prog. Theor. Phys.* **12** 421
Kunz A B 1972 *Phys. Rev.* B **6** 606

[18] Hedin L and Lundqvist S 1969 *Solid State Physics* vol 23, ed F Seitz, D Turnbull and H Ehrenreich (New York: Academic)

[19] Aryasetiawan F and Gunnarsson O 1998 *Rep. Prog. Phys.* **61** 237

[20] Rössler U 1976 *Rare Gas Solids* vol 1, ed M L Klein and J A Venables (New York: Academic)

[21] Lehnen A P and Bruch L W 1980 *Physica* A **100** 215

[22] Smith B L 1971 *The Inert Gases (Wykeham Science Series)* (London: Wykeham). The polarizability is obtained from experimental dielectric data and the Clausius–Mossotti relationship.

[23] Full details of the *ab initio* calculations on Ar will be published elsewhere.

[24] Baldereschi A and Tosatti E 1979 *Solid State Commun.* **29** 131

[25] Wooten F 1972 *Optical Properties of Solids* (New York: Academic)

[26] Nijboer B R A and de Wette F W 1957 *Physica* **23** 309

[27] Born M and Huang K 1954 *Dynamical Theory of Crystal Lattices* (Oxford: Clarendon)